Optical Materials 38 (2014) 161–166

Contents lists available at ScienceDirect

Optical Materials

journal homepage: www.elsevier.com/locate/optmat

Computed electronic and optical properties of SnO_2 under compressive stress

A. Miglio [a,*], R. Saniz [b], D. Waroquiers [a], M. Stankovski [a], M. Giantomassi [a], G. Hautier [a], G.-M. Rignanese [a], X. Gonze [a]

[a] Institute of Condensed Matter and Nanosciences - NAPS, Université catholique de Louvain, Chemin des étoiles 8, B-1348 Louvain-la-Neuve, Belgium
[b] CMT-group, Departement Fysica, Universiteit Antwerpen, Groenenborgerlaan 171, B-2020 Antwerpen, Belgium

ARTICLE INFO

Article history:
Received 28 August 2014
Received in revised form 7 October 2014
Accepted 13 October 2014
Available online 8 November 2014

Keywords:
Density functional theory
Transparent conducting oxides
Absorption spectrum
Tin dioxide

ABSTRACT

We consider the effects of three different types of applied compressive stress on the structural, electronic and optical properties of rutile SnO_2. We use standard density functional theory (DFT) to determine the structural parameters. The effective masses and the electronic band gap, as well as their stress derivatives, are computed within both DFT and many-body perturbation theory (MBPT). The stress derivatives for the SnO_2 direct band gap are determined to be 62, 38 and 25 meV/GPa within MBPT for applied hydrostatic, biaxial and uniaxial stress, respectively. Compared to DFT, this is a clear improvement with respect to available experimental data. We also estimate the exciton binding energies and their stress coefficients and compute the absorption spectrum by solving the Bethe–Salpeter equation.

1. Introduction

SnO_2 belongs to a class of post-transition-metal compounds such as ZnO and In_2O_3 that are typically used as transparent conducting oxides (TCOs). These TCOs are insulating oxides that by appropriate doping become conductive, still maintaining their transparency in the visible [1]. TCOs are used for photovoltaic solar cells, transparent electrodes, liquid crystal displays, smart windows, gas sensors and other optoelectronic devices. SnO_2 films are chemically and thermally stable, mechanically strong and rather inexpensive [2]. As a result, SnO_2 is one of the most used n-type TCO material. In order to exploit SnO_2 for new applications, a deep understanding of its key bulk properties is therefore necessary.

The naturally occurring form of stannic oxide (SnO_2) is the mineral cassiterite. It adopts the rutile structure with a tetragonal unit cell. It is a wide-gap semiconductor with optical gap around 3.6 eV [2]. Its properties can actually be engineered by applying an external pressure in order to intentionally deform its crystalline structure.

A few experimental [3–6] and computational [7–10] studies on the structural, electronic and optical properties of SnO_2 under pressure have been reported. First-principles electronic structure calculations on SnO_2 have been carried out with different methods, most of them in the framework of density functional theory (DFT) [11,12]. DFT has proven to be accurate for the description of structural properties of SnO_2. In contrast, it severly underestimates the value of the band gap, by at least 1.8 eV, and in the worst case by as much as 2.7 eV. Such a behavior is not surprising, as DFT with standard local or semi-local exchange–correlation (XC) functionals usually underestimates significantly the band gap [13,14]. More recently, many-body perturbation theory (MBPT) [13,14] was used to improve the description of SnO_2 excited-state properties [7,15–18]. Although most computations give results that are closer to the experimental data, there are still discrepancies up to 0.7 eV in the reported band gap values.

Experimental works available in the literature focused on the behavior of SnO_2 under high pressure, and different phase transitions have been described. However, there is a clear evidence that SnO_2 is stable in the rutile structure for pressures below ~12 GPa [3]. It should be noted that most of the available experimental measurements focus on the effect of hydrostatic pressure. For example, Schweitzer et al. [4] have investigated the effects of hydrostatic pressure on the fundamental gap, E_g, and on the exciton binding energy, E_B^{exc}, of bulk SnO_2 by performing two-photon absorption experiments at $T = 7$ K. In SnO_2, indeed, the direct optical transition from the valence band maximum (VBM) to the first conduction band minimum (CBM) is dipole forbidden while two-photon absorption is allowed. In their work, they have reported a band gap pressure coefficient, dE_g/dp, of 62.0 meV/GPa, an exciton binding energy of ~50 meV with a pressure coefficient, dE_B^{exc}/dp, of 0.87 meV/GPa.

* Corresponding author. Tel.: +32 10473694.
E-mail address: anna.miglio@uclouvain.be (A. Miglio).

http://dx.doi.org/10.1016/j.optmat.2014.10.017
0925-3467/

Contrary to the hydrostatic pressure, anisotropic stresses can lead to both compressive and tensile strains. These more selective stresses could thus be used in order to tune targeted properties of a material. During the growth process, crystals are often exposed to anisotropic and inhomogeneous mechanical stresses. Tensile and compressive stress fields are generated in the thin semiconductor layers. These phenomena occur in the lattice-mismatched heterostructures, in applications for flexible electronics or in materials with intrinsic or induced lattice defects. TCOs are usually deposited as thin films and therefore they are often subject to the biaxial strain induced by the substrate [19].

The behavior of the electronic band structure of SnO_2 under anisotropic (uniaxial) compressive stress has been studied previously by Saniz et al. [7] with DFT and MBPT using LDA, although relativistic corrections for Sn atom were neglected, and the effects of hydrostatic and biaxial stress on the optical properties were not considered. In the recent works by Cai et al. [20] and by Zhou et al. [10] the dependence of the electronic band structure and of the band gap on hydrostatic pressure and biaxial stress respectively, was computed *ab initio* with DFT.

In this paper, we extend the previous study of Saniz et al., by investigating the effects of hydrostatic pressure as well as of biaxial and uniaxial compressive stresses on SnO_2, up to 3 GPa [7].

In Section 2 we first summarize the theoretical and computational methods used in this work. In Sections 3 and 4, we present the structural deformations and the evolution of the electronic structure of SnO_2 under stress computed from first-principles with all-electron (AE) methods and a norm-conserving pseudopotential (PP) based approach. We use PP to compare the effects of DFT and MBPT on the fundamental band gap. Finally, in Section 5, we qualitatively discuss how the stress affects the optical properties of SnO_2 computed within the Bethe–Salpeter formalism (BSE) [14] and we estimate the stress coefficients of the excitonic binding energies.

2. Methods

In this paper, the pressure effects on the electronic and optical properties of SnO_2 are computed within DFT and MBPT. All the DFT calculations are performed both with the PP and AE approaches. In contrast, MBPT calculations are performed based on the PP formalism.

In all ground state calculations, the XC energy is described in the local-density approximation (LDA) using the Perdew-Wang functional [21].

PP calculations are performed with plane waves as implemented in the ABINIT code [22]. All PPs are generated with the Troullier–Martins scheme [23]. Sn $5p^2$, $5s^2$, $4d^{10}$, $4p^6$, $4s^2$ electrons and O $2s^2$, $2p^4$ electrons are treated as valence states and scalar relativistic corrections are included for Sn. In order to converge the band structure energies within 1 meV, an energy cutoff of 105 Ha has been used.

SnO_2 lattice parameters and electronic gap have been computed with various computational approaches, including PP, AE and the projector augmented wave (PAW) method where the use of a pseudized wavefunction is combined with atomic-like orbitals inside atom centered spheres to correctly describe the nodal shape of the wavefunction [24]. Table 1 summarizes the results obtained in this work and compare them with selected published results. We observe a significant variation in the band gap values, which we ascribe to the intrinsic inability of DFT to treat localized states such as Sn 4*d* and to the use of different PP. For this reason, we compare results obtained with PP and AE calculations as implemented in a full-potential linearized augmented-plane wave code [25]. We note that the results obtained by including relativistic effects in the Sn PP are closer to the AE results. This clearly indicates the importance of such correction and validates the set of pseudopotentials used in this work.

Table 1
SnO_2 lattice parameters and electronic gap computed within DFT using different methods and XC functionals. Our results are compared to other theoretical values and to the experimental data. For the electronic gap, the value obtained within MBPT is also indicated when available.

Method	Functional	Refs.	a (Å)	c (Å)	E_g^{DFT} (eV)	E_g^{MBPT} (eV)
PP	LDA	[26]	4.73	3.19	0.94	2.89
PP	LDA	[7]	4.72	3.19	1.80	3.85
PP	LDA	[15]	4.72	3.05	1.71	3.85
PAW	LDA	[5]	4.74	3.19	–	–
PAW	LDA(+U)	[18]	4.74	3.2	0.94	3.65
AE	LDA	[27]	4.76	3.18	1.08	–
PP	LDA	This work	4.72	3.19	0.89	2.75
AE	LDA	This work	–	–	1.17	–
Exp.		[3,28]	4.74	3.19	3.6	

In AE calculations the charge density is expanded in k-space up to G_{max} = 12 Bohr^{-1}. The cut-off value for the planewave expansion of the wave functions in the interstitial region (*i.e.* the value that defines the maximum length for the $G + k$ vectors) is *rgmax* = 8.

In order to simulate the applied pressure, the unit cell is optimized for each given stress using PP calculations with ABINIT. The non-diagonal components of the stress tensor are set to zero and thus non-shear stress only is taken into account. The compressive uniaxial stress $-\sigma_{\parallel}$ along the c axis (Fig. 1) is obtained imposing that the diagonal components of the stress tensor are $\sigma_{\parallel} = \sigma_{zz}$ and $\sigma_{xx} = \sigma_{yy} = 0$ where the z direction coincides with the c axis and is orthogonal to the *ab* plane (Fig. 1). An homogeneous compressive (biaxial) stress $-\sigma_{\perp}$ in the *ab* plane is simulated by setting the stress tensor component as $\sigma_{\perp} = \sigma_{xx} = \sigma_{yy}$ and $\sigma_{zz} = 0$. The hydrostatic pressure is indicated as $-\sigma_h$.

We also perform AE DFT calculations to compute the electronic structure of SnO_2, the density of states and the effective masses. In these calculations, only atomic positions are allowed to relax, while the cell parameters are fixed to the values obtained from the structural relaxation performed with PPs.

DFT represents a reliable method for computing structural properties whereas it usually fails in predicting excited state properties (like the band gap). Therefore, we employ MBPT to overcome the DFT band gap problem [13]. In solving Hedin's equations [31,13,14], the self-energy operator is obtained by the one-shot perturbative approach (G_0W_0) with the Godby-Needs plasmon-pole model [32], with the eigenvalues and wave functions computed either within DFT or from the self-consistent Coulomb-hole screened-exchange approximation (scCOHSEX) [31,33].

All LDA calculations with PP are performed on a shifted $4 \times 4 \times 6$ Monkhost–Pack (MP) [34] grid. For MBPT calculations, we use a $4 \times 4 \times 6$ MP grid. The screened interaction W is computed on a $(\frac{1}{2}, \frac{1}{2}, \frac{1}{2})$ shifted mesh and the self-energy operator is evaluated on

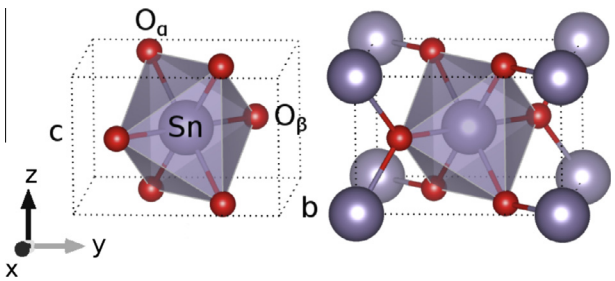

Fig. 1. SnO_2 rutile (space-group symmetry $P4_2/mnm$) unit cell, containing two formula units. Oxygen atoms form a distorted octahedron around each tin atom. The Sn–O octahedral coordination is illustrated in the left panel where subscripts on oxygen atom indicate inequivalent Sn–O bonds.

a Γ-centered grid. The cut-off energies for the wave functions and the dielectric matrix, as well as the number of empty states included in the calculations allow us to converge the quasiparticle eigenenergies within 0.05 eV. The elastic constants are computed on a $10 \times 10 \times 15$ MP grid.

We compute the charge carriers effective masses from DFT via parabolic fit of the band structures near the CBM and VBM at the Γ point, along the directions parallel (Γ–X) and orthogonal (Γ–Z) to the c-axis, respectively. The optical absorption spectra are computed both in the random phase approximation (RPA) and including the electron–hole interaction via the solution of the Bethe–Salpeter equation. The BSE is solved including local field effects, and approximating W with a model dielectric function [35] constructed from the electronic dielectric constant ϵ_∞ computed in the RPA. This approximation was validated in the $-\sigma_\parallel$ case by comparing the model dielectric function results with those obtained with the *ab initio* W from a G_0W_0 calculation. It is found that the spectra are very similar in the energy range of interest. It is worth stressing that the sampling of the Brillouin zone is improved by adding a small shift to the grid of k-points, along a symmetry breaking direction.

3. Structural properties

SnO_2 crystallizes in the rutile structure with a tetragonal unit cell (space group $P4_2/mnm$) characterized by lattice parameters $a = b = 4.738$ Å and $c = 3.188$ Å (see Ref. [3]). The internal parameter u is $\sim$0.307.

The structural parameters at equilibrium, computed within LDA, ($a = 3.185$ Å, $c = 4.719$ Å, and $u = 0.306$) are in good agreement with previously published results (see Table 1) and experimental values [5,7,18,26].

In the rutile unit cell, Sn atoms are octahedrally coordinated to the 6 oxygen nearest neighbors (Fig. 1). The Sn atoms are located at Wyckoff sites 2(a), corresponding to reduced coordinates $(0,0,0)$ and $(1/2,1/2,1/2)$, while the four O atoms sit at the 4(f) sites $(\pm u, \pm u, 0)$ and $(1/2 \pm u, 1/2 \mp u, 1/2)$.

In the left panel of Fig. 1, we consider the environment of the central Sn atom. We label the two inequivalent oxygen atoms relative to this central Sn atom as O_α and O_β. The octahedron deformation is defined by the ratio of the $\overline{SnO_\alpha}$ and $\overline{SnO_\beta}$ distances and by the angle $O_\alpha\widehat{SnO}_\beta$.

The effect of the applied (hydrostatic) stress on the lattice parameters is presented in Fig. 2, and compared with available experimental data from Haines et al. [3]. In Table 2, we compare the bulk-modulus of SnO_2 computed with PP and AE techniques. The results agree with each other within 3%.

The pressure-induced change in the structural parameters is almost linear. The pressure coefficients obtained with a linear least-squares fit are reported in Table 3, as well as the coefficients relative to the internal variation in Sn–O distances. The same methodology is used to obtain the pressure coefficients for non-hydrostatic stresses, also reported in the same table. Our results agree well with previous published calculations [5].

The lattice deformation is directly related to the elastic constants. In Table 2, we compare our results for the elastic constants with available experimental data. Our data are within the range of variation of the experimental values and of previously published *ab initio* results [7,8,30]. It should be noticed that the LDA results are in much better agreement with the experimental data than the corresponding GGA results.

4. Electronic structure

Fig. 3 displays the upper valence bands and the lowest conduction bands, in the energy range from -10 to 6 eV (the zero of energy is located at the VBM). The partial density of states (PDOS) at equilibrium is also reported. The conduction band consists essentially of Sn 5s and Sn 5p orbitals while O 2s states have little contribution. The upper valence bands are mainly due to O 2p and Sn 5p-4d orbitals, while in the -6 to -8 eV range O 2p hybridize with Sn 5s states. Other valence bands, lower in energy (not shown in Fig. 3) arise from the O 2s and Sn 4d states. It is found that the main features of the LDA and GGA band structures are similar to each other and consistent with previous results.

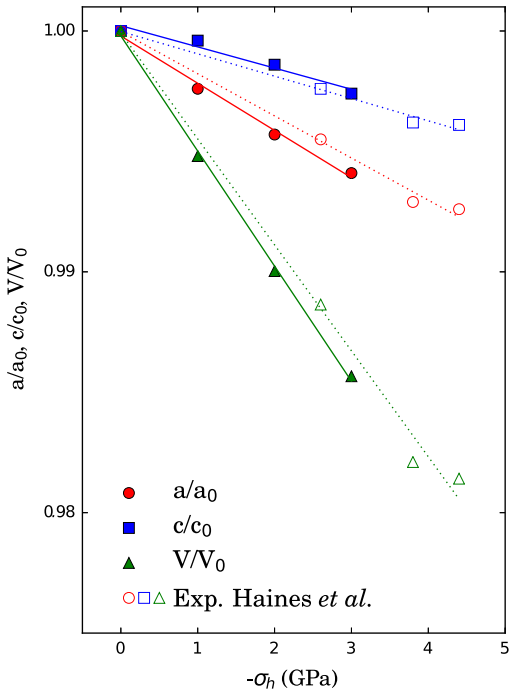

Fig. 2. The unit cell parameters a and c of SnO_2 under hydrostatic pressure σ_h. Open symbols refer to experimental data from Haines and Léger [3].

As expected, the valence and conduction bands are mainly of bonding and antibonding character and $\sigma_\parallel$ tends to increase the bonding-antibonding split. Besides increasing the band gap, pressure mainly affects the valence states located in the energy window from -4 to -6 eV.

Available experimental results for SnO_2 electronic properties are often difficult to interpret due to the quality of the sample that depends on the growth and deposition conditions, and on the post-deposition treatment [39]. There are no reported measurements of SnO_2 electronic band gap from photoemission experiments, but the fundamental direct gap has a lower limit defined by the direct optical gap (3.6 eV) [28]. SnO_2 presents a single free-electron-like conduction band minimum, similar to In_2O_3 and ZnO. The effective mass model is therefore justified, and cyclotron resonance experiments give electron effective masses $\leqslant 0.3 m_0$ [37].

Although the absolute value of the DFT–LDA band gap is not reliable, it is meaningful to compare the derivatives of the band gap with respect to the total pressure. Previous studies have shown that the DFT band gap pressure derivatives are quite accurate and with no significant dependence on the different XC functionals [40,41].

Both the DFT (PP and AE) and the MBPT approximations predict this relationship to be linear (see Fig. 4), but the slopes differ. Despite the difference in the absolute values of the LDA gaps, AE and PP predict band gap pressure coefficients that differ by less than 1 meV/GPa. The results obtained with MBPT are found in much better agreement with the experimental data than DFT. On the other hand, it is worth noticing that while DFT–LDA

Table 2
SnO_2 elastic tensor components and bulk modulus (GPa) at 0 GPa calculated within DFT using different methods and XC functionals. Our results are compared to other theoretical values and to the experimental data measured at ambient conditions from Ref. [29].

Method	Functional	Ref.	$c_{11} = c_{22}$	c_{33}	c_{12}	c_{13}	c_{44}	c_{66}	B
PP	LDA	[7]	274.3	412.5	180.9	149.8	94.3	202.9	211.7
PAW	GGA	[30]	246.6	459.6	183.4	156.5	97.4	203.3	199.3
PP	LDA	This work	249	430	177	155	95	205	199
AE	LDA	This work	–	–	–	–	–	–	193
Exp.		[29]	261.7	449.6	177.2	155.5	103.1	207.4	212.3

Table 3
Stress coefficients d/dp relative to several structural parameters, with respect to the different types of stress, computed with LDA.

(10^{-2} Å/GPa)	$-\sigma_\perp$	$-\sigma_\parallel$	$-\sigma_h$
da/dp	−1.51	0.51	−0.92
dc/dp	0.74	−0.93	−0.28
d$\overline{SnO_\alpha}$/dp	−0.29	0.07	−0.22
d$\overline{SnO_\beta}$/dp	−0.61	0.14	−0.44

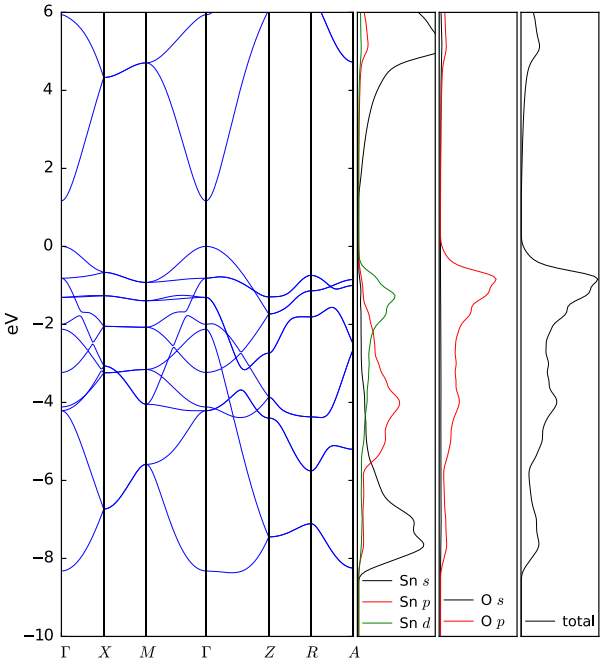

Fig. 3. Band structure and the projected density of states in LDA at equilibrium (0 GPa).

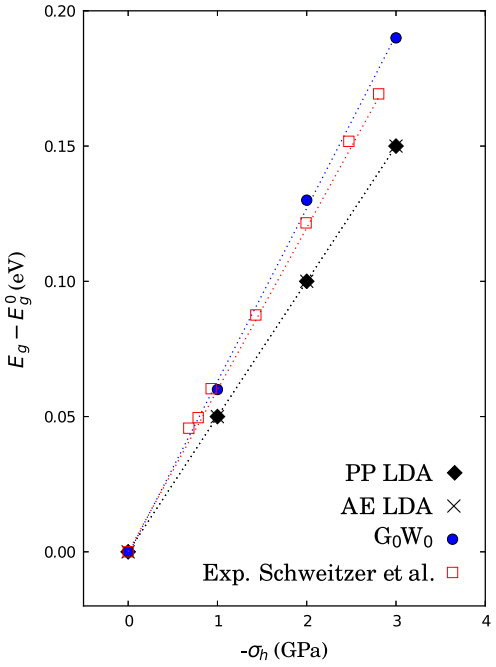

Fig. 4. The effects of σ_h on the band gap of SnO_2. We report values obtained with LDA (PP and AE) and G_0W_0 calculations.

underestimates the absolute value of the gap by ∼70%, the LDA underestimation for the band gap change rate reduces to ∼20%.

Building upon this validation of the G_0W_0 methodology, we carry on, and obtain the pressure coefficient for the fundamental band gap, for the different types of stress, by a least square fit assuming a linear dependence of the band gap. The tetragonal symmetry of the crystal structure of SnO_2 leads to an anisotropy in the electronic and optical properties. For example, the smaller distance between Sn atoms along the c-axis, may facilitate a higher atomic orbital overlap and thus a more conductive pathway for electron transport. For example, rutile TiO_2 conductivity is five to ten times greater along the c-axis as compared to the ⟨1 1 0⟩ direction [42].

The band gap stress coefficients are reported in Table 5. Those relative to $\sigma_\parallel$ are comparable to those of similar semiconductors, such as TiO_2. Table 5 shows that, in terms of efficiency in tuning SnO_2 band gap, the hydrostatic stress is the most effective, while purely uniaxial stress is the least. This is consistent with the recent results reported in Ref. [10] in which the authors discuss the effect of biaxial stress in the bc plane of SnO_2 (at variance with our ab biaxial stress). Zhou et al. computed the band gap pressure coefficient within DFT using the HSE functional. They obtained a value of 46 meV/GPa confirming that biaxial stress is the most suitable for tuning tin oxide band gap.

Despite being an excited state property, the effective masses from DFT–LDA are quite close to experimental data, as shown in Table 4. Due to numerical issues related to k-point sampling, computing effective masses from MBPT is more difficult than from DFT. Given the reasonably good agreement of the DFT data with experiment, we will rely on it for the pressure dependence of the effective masses. The dependence of the effective mass on pressure is reported in Table 5 and are extremely small. Regardless of the method, whether PP or an AE approach, electron effective mass changes by few percent *e.g.* when uniaxial stress is applied the change is ∼0.01 per GPa along directions orthogonal to the c-axis and 0.001 per GPa along a direction parallel to c.

5. Optical properties

We are interested in the effect of stress on the optical properties and particularly on the optical gap. In principle, we should compute all dielectric functions by solving the BSE and hence take excitonic effects into account.

Table 4
SnO_2 electron and hole effective masses at Γ computed with different theories (DFT or MBPT), methods, and XC functionals. Our results are compared to other theoretical values.

Method	Theory	Functional	Ref.	m_e^*		m_h^*	
				$\Gamma-Z$	$\Gamma-M$	$\Gamma-Z$	$\Gamma-M$
PP	DFT	LDA	[7]	0.223	0.253	1.655	1.228
PAW	MBPT	HSE[a]	[18]	0.21	0.26	1.47	1.21
PAW	DFT	HSE	[36]	0.21	0.25	1.60	1.27
PP	DFT	LDA	This work	0.18	0.21	1.67	1.23
Exp.			[37]	0.234	0.299	–	–

[a] Ref. [38].

Table 5
Stress coefficients d/dp relative to the band gap and the effective masses, with respect to the different types of stress, computed with LDA, G_0W_0 and scCOHSEX+G_0W_0. For the effective mass parameters, only the LDA data have been computed.

Method	dE_g/dp (meV/GPa)		
	$-\sigma_\perp$	$-\sigma_\parallel$	$-\sigma_h$
LDA	32	20	51
G_0W_0	38	25	62
scCOHSEX+G_0W_0	–	27	–
Exp.	–	–	62[a]
(m_0/GPa) dm_e^*/dp			
$\Gamma-Z$	0.001	0.001	0.002
$\Gamma-M$	−0.029	0.017	−0.014
dm_h^*/dp			
$\Gamma-Z$	∼ 0	0.003	0.003
$\Gamma-M$	−0.002	−0.003	−0.004

[a] Ref. [4].

By linearly extrapolating the slope of the absorption curves around the half maximum of the onset to zero absorption, we obtain the optical gaps. However, the computational cost required to converge the BSE spectra around the absorption onset is extremely high because of the slow convergence with respect to the *k*-point sampling. Here we report on BSE results for the case of uniaxial stress only (see Fig. 5). As noted before, the rutile SnO_2 has a tetragonal symmetry and therefore only two components of the dielectric function are independent. In Fig. 5, the absorption spectra i.e. the imaginary part of ε is plotted in the ordinary ($\varepsilon_\perp$) and extraordinary ($\varepsilon_\parallel$) polarization. The applied pressure has stronger effects on the absorption onset for light polarization parallel to the *c*-axis, the anisotropy is apparent.

The computed spectra reported in Fig. 5 reveal significant excitonic effects. For instance, a sharper absorption onset is obtained compared to RPA calculations. The dielectric function shows significant anisotropy between its components perpendicular and parallel to the *c*-axis. A pronounced excitonic peak is visible around the absorption onset of the perpendicular component. Our calculated static refraction indices differ by ∼0.1, in agreement with the experimentally observed birefringence in SnO_2 (and TiO_2).

Solving the BSE should in principle give the value of the binding energies of excitons. In consideration of the computational cost of the BSE, we resort to the two-band model of Wannier-Mott [43,44] in order to obtain a qualitative description of the excitonic binding energies for the three types of stress. One can approximate the binding energy of the first exciton as $E_B^{exc} = R_\infty \mu / m_e \varepsilon_{eff}^2$, where μ is the reduced effective mass and ε_{eff} is the effective static screening. Indeed, we have previously assumed that the parabolic approximation can be applied to the dispersion of SnO_2 highest valence and lowest conduction band. The Wannier-Mott approximation, in the case of materials similar to SnO_2, has been reported

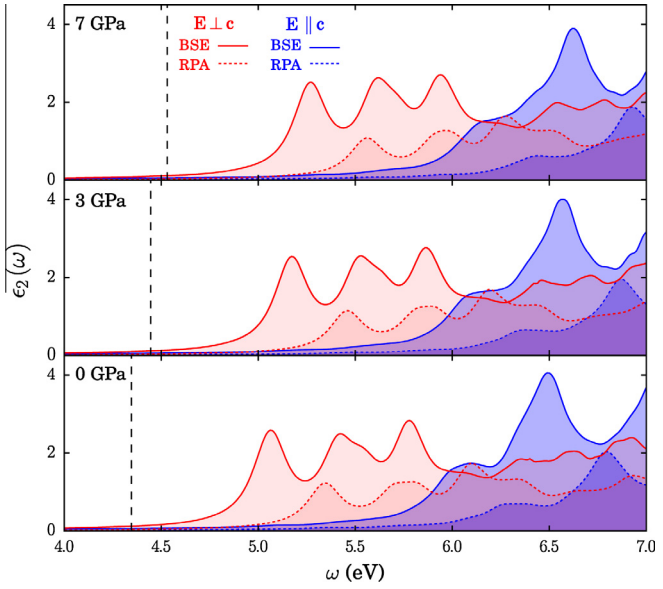

Fig. 5. The imaginary part of the dielectric function, close to the absorption edge computed within RPA (dotted line) and solving the BSE (solid line). The spectra are computed at zero pressure (lower panel) and for an applied compressive uniaxial stress $\sigma_\parallel$ ∼3 GPa (central panel) and ∼7 GPa (upper panel). Red (blue) curves are relative to the light polarization perpendicular (parallel) to the *c* axis of the rutile structure. We correct the LDA band gap with a rigid shift to match the scCOHSEX+G_0W_0 values (vertical dotted lines). (For interpretation of the references to colour in this figure legend, the reader is referred to the web version of this article.)

to give excitonic binding energies in agreement with BSE results [44].

We use the $\varepsilon_\infty^\perp$ computed within the RPA approach (Table 6) and the carriers effective masses to compute the excitonic binding energies E_B^{exc} presented in Table 6. The E_B^{exc} at equilibrium ($\sigma = 0$) is 157 (146) meV for the ordinary $E \perp c$ ($E \parallel c$ extraordinary) polarization.

It is known that computed excitonic binding energies can overestimate the experimental value by up to one order of magnitude. The experimental excitonic binding energy of SnO_2 is ∼30–50 meV [28,4]. The large discrepancy with respect to the experimental values can be ascribed to the incorrect description of the screening.

Indeed, as illustrated in Ref. [18], if we take the average of the experimental static dielectric constants of SnO_2 *i.e.* $\varepsilon_0^\perp = 14$ and $\varepsilon_0^\parallel = 9$ [45] and compute the Wannier-Mott exciton binding energies we obtain $E_B^{exc} \sim 20$ meV.

In light of the above discussion, it is expected that the dE_B^{exc}/dp experimental value [4] relative to hydrostatic pressure is overestimated by our calculations.

Table 6
Macroscopic dielectric constant ε_∞ under hydrostatic pressure and biaxial, uniaxial stress, computed within the RPA. The computed ε_∞ at zero pressure is 3.92 (4.02 AE FP-LAPW). Excitonic binding energy E_B^{exc} and binding energy pressure coefficients dE_B^{exc}/dp for the different types of stress (σ_{ii} = 3 GPa), computed within the Wannier-Mott approximation.

	$-\sigma_\perp$	$-\sigma_\parallel$	$-\sigma_h$
ε_∞	3.86	3.81	3.83
E_B^{exc} (meV)			
$E \perp c$	162	183	170
$E \parallel c$	152	167	158
dE_B^{exc}/dp (meV/GPa)			
$E \perp c$	1.6	7.7	4.4
$E \parallel c$	1.7	6.0	3.8

6. Summary and conclusions

In this paper, we have investigated the effect of pressure on the structural, electronic and optical properties of rutile SnO_2. The resulting trends for the fundamental band gap, the band dispersion, and the electron effective masses under pressure are comparable to the experimental findings for similar compounds *e.g.* TiO_2. The use of different DFT implementations does not influence significantly the effect of pressure on the band gap. As reported in Refs. [46,47], for some simple semiconductors, the LDA band gap pressure coefficients are very close to the quasiparticle values, obtained via G_0W_0.

However, the pressure coefficient for the hydrostatic pressure computed with G_0W_0 is in better agreement with the experimental result of Schweitzer et al. [4] compared to DFT. Our calculations indicate that hydrostatic pressure is the most effective among the different types of stress for tuning the SnO_2 band gap.

In addition, we compute exciton binding energies and their corresponding stress coefficients and we present the optical absorption spectra. We show that the impact of excitonic effects is significant and has to be taken into account in the calculations *e.g.* by solving the BSE.

Acknowledgements

This work was supported by the FRS-FNRS through a FRIA grant (D.W.) and a FNRS grant (G.H.). This work was also supported by the IWT Project Number 080023 (ISIMADE), the Région Wallonne through WALL-ETSF project Number 816849, the EU-FP7 HT4TCOS Grant No. PCIG11-GA-2912–321988, the FRS-FNRS through contracts FRFC Number 2.4.589.09.F and AIXPHO (PDR Grant T-0238.13). The authors would like to thank Yann Pouillon and Jean-Michel Beuken for their valuable technical support and help with the test and build system of ABINIT. Computational resources have been provided by the supercomputing facilities of the Université catholique de Louvain (CISM/UCL) and the Consortium des Equipements de Calcul Intensif en Fédération Wallonie Bruxelles (CECI) funded by the Fonds de la Recherche Scientifique de Belgique (FRS-FNRS) under Grant No. 2.5020.11.

References

[1] D.S. Ginley, H. Hosono, D.C. Paine, Handbook of Transparent Conductors, Springer, 2010.
[2] M. Batzill, U. Diebold, The surface and materials science of tin oxide, Prog. Surf. Sci. 79 (2005) 47.
[3] J. Haines, J.M. Léger, X-ray diffraction study of the phase transitions and structural evolution of tin dioxide at high pressure: relationships between structure types and implications for other rutile-type dioxides, Phys. Rev. B 55 (1997) 11144.
[4] C. Schweitzer, K. Reimann, M. Steube, Two-photon spectroscopy of SnO_2 under hydrostatic pressure, Solid State Commun. 110 (1999) 697–700.
[5] K. Parlinski, Y. Kawazoe, Ab initio study of phonons in the rutile structure of SnO_2 under pressure, Eur. Phys. J. B 13 (2000) 679–683.
[6] Y. Li, W. Fan, H. Sun, et al., Optical properties of the high-pressure phases of SnO_2: first-principles calculation, J. Phys. Chem. A 114 (2010) 1052–1059.
[7] R. Saniz, H. Dixit, D. Lamoen, B. Partoens, Quasiparticle energies and uniaxial pressure effects on the properties of SnO_2, Appl. Phys. Lett. 97 (2010) 261901. In this work the reported value of the uniaxial pressure (3.1 GPa) corresponds to $-\sum\sigma_{ii}/3$ where $\sigma_{xx}=\sigma_{yy}=0\sigma_{zz}\approx$10 GPa.
[8] C.-M. Liu, X.-R. Chen, G.-F. Ji, First-principles investigations on structural, elastic and electronic properties of SnO_2 under pressure, Comp. Mater. Sci. 50 (2011) 1571–1577.
[9] K. Liu, M. Sakurai, M. Aono, Controlling semiconducting and insulating states of SnO_2 reversibly by stress and voltage, ACS Nano 6 (2012) 7209–7215.
[10] W. Zhou, Y. Liu, Y. Yang, P. Wu, Band gap engineering of SnO_2 by epitaxial strain: experimental and theoretical investigations, J. Phys. Chem. C 118 (2014) 6448–6453.
[11] P. Hohenberg, W. Kohn, Inhomogeneous electron gas, Phys. Rev. 136 (1964) B864.
[12] W. Kohn, L. Sham, Self-consistent equations including exchange and correlation effects, Phys. Rev. (1965) A1133.
[13] W.G. Aulbur, L. Jönsson, J.W. Wilkins, Solid state physics volume, Solid State Physics, vol. 54, Elsevier, 1999.
[14] G. Onida, L. Reining, A. Rubio, Electronic excitations: density-functional versus many-body green's-function approaches, Rev. Mod. Phys. 74 (2002) 601.
[15] M. Palummo, L. Reining, M. Meyer, C. Bertoni, in: D.J. Lockwood (Ed.), 22nd Intern. Conf. on the Phys. of Semicond, LNCS, vol. 5805, World Scientific, Singapore, 1995.
[16] C. Sevik, C. Bulutay, High dielectric constant and wide band gap inverse silver oxide phases of the ordered ternary alloys of SiO_2, GeO_2, and SnO_2, Phys. Rev. B 74 (2006) 193201.
[17] J. Berger, L. Reining, F. Sottile, Ab initio calculations of electronic excitations: collapsing spectral sums, Phys. Rev. B 82 (2010) 041103. R.
[18] A. Schleife, J. Varley, F. Fuchs, C. Rödl, F. Bechstedt, P. Rinke, A. Janotti, C. Van de Walle, Tin dioxide from first principles: quasiparticle electronic states and optical properties, Phys. Rev. B 83 (2011) 035116.
[19] A. Walsh, C. Catlow, K. Zhang, R. Egdell, Control of the band-gap states of metal oxides by the application of epitaxial strain: the case of indium oxide, Phys. Rev. B 83 (2011) 161202. R.
[20] L.-G. Cai, F.-M. Liu, D. Zhang, W.-W. Zhong, The influence of hydrostatic pressure on the electronic structure and optical properties of tin dioxide: a first-principle study, Phys. B: Condensed Matter 408 (2013) 73.
[21] J.P. Perdew, Y. Wang, Accurate and simple analytic representation of the electron-gas correlation energy, Phys. Rev. B 45 (1992) 13244.
[22] X. Gonze et al., ABINIT: first-principles approach to material and nanosystem properties, Comput. Phys. Commun. 180 (2009) 2582–2615.
[23] N. Troullier, J. Martins, Efficient pseudopotentials for plane-wave calculations, Phys. Rev. B 43 (1991) 1993.
[24] P. Blöchl, Projector augmented-wave method, Phys. Rev. B 50 (1994) 17953.
[25] ELK, FP-LAPW code. <http://elk.sourceforge.net>, 2013.
[26] J. Berger, L. Reining, F. Sottile, Efficient GW calculations for SnO_2, ZnO, and rubrene: the effective-energy technique, Phys. Rev. B 85 (2012) 085126.
[27] E. Peltzer y Blancá, A. Svane, N. Christensen, C. Rodríguez, O. Cappannini, M. Moreno, Calculated static and dynamic properties of β-Sn and Sn–O compounds, Phys. Rev. B 48 (1993) 15712–15718.
[28] K. Reimann, M. Steube, Experimental determination of the electronic band structure of SnO_2, Solid State Commun. 105 (1998) 649.
[29] E. Chang, K. Graham, The elastic constants of cassiterite SnO_2 and their pressure and temperature dependence, J. Geophys. Res. 80 (1975) 2595–2599.
[30] W. Miiller, G.J. Kearley, C.D. Ling, Ab initio parametrized polarizable force field for rutile-type SnO_2, Theor. Chem. Acc. 131 (2012) 1216.
[31] L. Hedin, New method for calculating the one-particle Green's function with application to the electron-gas problem, Phys. Rev. 139 (1965) A796.
[32] R. Godby, R. Needs, Metal-insulator transition in Kohn-Sham theory and quasiparticle theory, Phys. Rev. Lett. 62 (1989) 1169.
[33] F. Bruneval, N. Vast, L. Reining, Effect of self-consistency on quasiparticles in solids, Phys. Rev. B 74 (2006) 045102.
[34] H. Monkhorst, J. Pack, Special points for Brillouin-zone integrations, Phys. Rev. B 13 (1976) 5188.
[35] F. Bechstedt, R. Del Sole, G. Cappellini, L. Reining, An efficient method for calculating quasiparticle energies in semiconductors, Solid State Commun. 84 (1992) 765.
[36] M. Dou, C. Persson, Comparative study of rutile and anatase SnO_2 and TiO_2: band-edge structures, dielectric functions, and polaron effects, J. Appl. Phys. 113 (2013) 083703.
[37] J. Button, C. Fonstad, W. Dreybrodt, Determination of the electron masses in stannic oxide by submillimeter cyclotron resonance, Phys. Rev. B 4 (1971) 4539–4542.
[38] J. Heyd, G. Scuseria, M. Ernzerhof, Hybrid functionals based on a screened coulomb potential, J. Chem. Phys. 118 (2003) 8207.
[39] J. Robertson, B. Falabretti, Electronic structure of transparent conducting oxides, in: D.S. Ginley, H. Hosono, D.C. Paine (Eds.), Handbook of Transparent Conductors, Springer, 2010.
[40] K. Chang, S. Froyen, M.L. Cohen, Pressure coefficients of band gaps in semiconductors, Solid State Commun. 50 (1984) 105–107.
[41] N.E. Christensen, Electronic structure of GaAs under strain, Phys. Rev. B 30 (1984) 5753–5765.
[42] O. Byl, J. Yates, Anisotropy in the electrical conductivity of rutile TiO_2 in the (1 1 0) plane, J. Phys. Chem. B 110 (2006) 22966.
[43] F. Bassani, G. Pastori Parravicini, Electronic and Optical Transitions in Solids, Pergamon Press, 1975.
[44] F. Fuchs, C. Rödl, A. Schleife, F. Bechstedt, Efficient $O(N^2)$ approach to solve the Bethe-Salpeter equation for excitonic bound states, Phys. Rev. B 78 (2008) 085103.
[45] H. van Daal, The static dielectric constant of SnO_2, J. Appl. Phys. 39 (1968) 4467.
[46] S. Fahy, K.J. Chang, S.G. Louie, M.L. Cohen, Pressure coefficients of band gaps of diamond, Phys. Rev. B 35 (1987) 5856–5859.
[47] X. Zhu, S. Fahy, S.G. Louie, Ab initio calculation of pressure coefficients of band gaps of silicon: comparison of the local-density approximation and quasiparticle results, Phys. Rev. B 39 (1989) 7840–7847.